Naval Research Laboratory

Washington, DC 20375-5320

NRL/MR/6756--93-7406

Implementation of a Compact Magnetic Electron Energy Spectrometer for Intense Relativistic Electron Beams

J. A. Gregor

University of Maryland
Laboratory for Plasma Research
College Park, MD

J. A. Antoniades

Charged Particle Physics Branch
Plasma Physics Division

November 5, 1993

REPORT DOCUMENTATION PAGE

Form Approved
OMB No. 0704-0188

1. AGENCY USE ONLY (*Leave Blank*)	2. REPORT DATE	3. REPORT TYPE AND DATES COVERED
	November 5, 1993	Interim

4. TITLE AND SUBTITLE

Implementation of a Compact Magnetic Electron Energy Spectrometer for Intense Relativistic Electron Beams

5. FUNDING NUMBERS

PE -61153N

6. AUTHOR(S)

J.A. Gregor* and J.A. Antoniades

7. PERFORMING ORGANIZATION NAME(S) AND ADDRESS(ES)

Naval Research Laboratory
Washington, DC 20375-5320

8. PERFORMING ORGANIZATION REPORT NUMBER

NRL/MR/6756--93-7406

9. SPONSORING/MONITORING AGENCY NAME(S) AND ADDRESS(ES)

Office of Naval Research
800 North Quincy Street
Arlington, VA 22217-5660

10. SPONSORING/MONITORING AGENCY REPORT NUMBER

11. SUPPLEMENTARY NOTES

*University of Maryland, Laboratory for Plasma Research
College Park, Maryland 20742

12a. DISTRIBUTION/AVAILABILITY STATEMENT

Approved for public release; distribution unlimited.

12b. DISTRIBUTION CODE

13. ABSTRACT (*Maximum 200 words*)

A diagnostic used for measuring the energy of 1 to 5 MEV pulsed electron beams by means independent of the beam generating device is investigated. The method employed is capable of collecting the required data optically in a single pulse. The beam energy is measured using a magnetic electron spectrometer coupled with a scintillating material. Using a polaroid camera to collect data, the energy of electron beams from two field emission diode accelerators is measured. The first is a nominal 1 MEV, 16 kA, 25 ns FWHM electron beam and the second is a nominal 5 MEV, 20 kA, 50 ns FWHM electron beam. A detailed study of measurement accuracy and possible sources of error was accomplished.

14. SUBJECT TERMS

Energy Relativistic Electron beam
Electron
Spectrometer

15. NUMBER OF PAGES

23

16. PRICE CODE

17. SECURITY CLASSIFICATION OF REPORT	18. SECURITY CLASSIFICATION OF THIS PAGE	19. SECURITY CLASSIFICATION OF ABSTRACT	20. LIMITATION OF ABSTRACT
UNCLASSIFIED	UNCLASSIFIED	UNCLASSIFIED	UL

NSN 7540-01-280-5500

Standard Form 298 (Rev. 2-89)
Prescribed by ANSI Std 239-18
298-102

CONTENTS

IMPLEMENTATION OF A COMPACT MAGNETIC ELECTRON ENERGY SPECTROMETER FOR INTENSE RELATIVISTIC ELECTRON BEAMS

I. INTRODUCTION

In order to understand the propagation of charged particle beams, knowledge of the beam energy is required. A number of methods are available to measure the energy of intense relativistic electron beams (IREB's) including energy range,[1,2] particle scattering, spectrometry, and calculation based on accelerator characteristics. For a pulsed IREB a compact magnetic electron spectrometer[3,4] has been proposed. This would allow both time resolved and time integrated measurement of beam energy in a single pulse using photographic data collection techniques. A magnetic electron beam energy analyzer capable of fitting inside eight-inch vacuum hardware was constructed[5] at the University of Maryland, Laboratory for Plasma Research. This device was used at the Naval Research Laboratory on the 1 MeV, 16 kA, 25 ns (FWHM) pulsed electron beam produced by Pulserad[6] and the 5 MeV, 20 kA, 35 ns (FWHM) pulsed electron beam produced by SuperIBEX.[6] Both accelerators produce electron beams by field emission from a beam diode driven by a Blumlein type pulse forming line. Analysis techniques for making accurate, reproducible measurements were developed, and a comprehensive error analysis was conducted to determine the accuracy of the device.

II. DESCRIPTION

The Energy Analyzer is composed of a box-shaped keeper made from high permeability magnetic iron lined with 26 Samarium Cobalt magnets, a stainless steel face plate and collimator, and a 2.5 cm thick graphite shield.[1] The magnets create a nominal 4.5 kGauss magnetic field within the keeper. An electron beam input to the device will first pass through a slit in a graphite shield (used to protect the device from damage due to high energy electrons). It is then collimated and enters the keeper where it will be influenced by a magnetic field to impact on a strip of NE 104 scintillator material. The side of the keeper opposite the collimator is open to allow observation of the light given off by the

Manuscript approved September 24, 1993.

scintillator when excited by the energetic electrons. Figure 1 shows a cutaway drawing of the energy analyzer.

A back-lit graticule is carved into the scintillator to allow rough measurement of beam energy directly from the digitized photographs. The graticule lines range from 1 to 5 MeV at $^1/_2$ MeV intervals. A separate fiducial line, well outside the design range of 1 to 5 MeV, acts as a reference. This line appears at the 6.25 MeV position, 100 mm from the collimator slit, and is back-lit from a source independent from that used to illuminate the graticule. This allows the graticule and the reference fiducial to be used separately or together, as desired. The experimental setup is shown in Figure 2.

III. THEORY OF OPERATION

The equation of motion for electrons in an electromagnetic field is given by

$$\frac{d\vec{p}}{dt} = e\cdot\left(\vec{E} + \vec{v}\times\vec{B}\right). \tag{1}$$

Inside the keeper E=0, B=B_z, and v=$r\dot{\theta}$ ($\dot{r} = \dot{z} = 0$). The equations of motion in cylindrical coordinates reduce to

$$-\gamma m r\dot{\theta}^2 = -er\dot{\theta}B_z \tag{2a}$$

$$\frac{d}{dt}\left(\gamma m r^2\dot{\theta}\right) = 0. \tag{2b}$$

Using (2a) and $v = \beta c$ we find a formula for the cyclotron radius of the electrons in the keeper, given by

$$r_c = \frac{\beta c}{\dot{\theta}} = \frac{\gamma m}{eB_z}\beta c \tag{3}$$

The input collimator forms a sheet beamlet that will perform one half of a cyclotron orbit (due to the constant magnetic field inside the keeper) before impacting the scintillator. Using conservation of energy we can express the relativistic factor in terms of electron beam energy,

$$E_T = mc^2 + eV = \gamma mc^2 \tag{4}$$

where β and γ are related by,

$$\gamma = \frac{1}{\sqrt{1-\beta^2}} = 1 + \frac{eV}{mc^2} \tag{5}$$

Equations (3), (4), and (5) can be combined to find an expression for the distance d_c between the collimator gap and the point on the scintillator impacted by a sheet beamlet with a kinetic energy E (in electron volts),

$$d_c = 2r_c = \frac{mc}{eB_z}\sqrt{\left(1 + \frac{E}{mc^2}\right)^2 - 1} \tag{6}$$

IV. ENERGY ANALYSIS TECHNIQUE

The first step in the analysis is to digitize a photograph of the scintillator with the reference fiducial and graticule simultaneously illuminated. With this information the energy scale can be set.

The curve of cyclotron radius vs energy is very nearly linear for energies significantly above the electron rest energy. A linear least squares fit may be performed on the curve of electron orbit diameter ($d_c = 2\ r_c$) vs energy within the range of interest (1 to 5 MeV). The slope of this line will yield a constant that can be used for energy vs distance conversion. The results of such a fit for this device are shown in Table 1.

d_c (mm)	Energy found using d_c (MeV)	Energy found from Fit (MeV)	Deviation (KeV)
0.0	0.0	-0.420	-419.69
12.931	0.5	0.440	-59.531
21.075	**1.0**	0.982	-17.771
28.825	**1.5**	1.498	-2.268
36.433	**2.0**	2.004	3.792
43.972	**2.5**	2.505	5.314
51.474	**3.0**	3.004	4.293
58.951	**3.5**	3.502	1.700
66.413	**4.0**	3.998	-1.934
73.865	**4.5**	4.494	-6.293
81.308	**5.0**	4.989	-11.179
100.00	**6.25**	6.25	0

Table 1 Theoretical cyclotron diameter and linear fit vs energy.

The energy vs distance conversion for this device was found to be 66.52 KeV/mm and is fixed due to the magnetic field strength and geometry. A conversion for energy vs pixel is obtained by dividing the energy difference between the reference fiducial and the 1 MeV graticule line by the distance in pixels between these two points on the digitized image. This is dependent on how the image is digitized. These two pieces of information allow us to find the distance vs pixel conversion and magnification factor of our experimental setup. For this experiment the digitized distance between the 1 MeV line and the reference graticule was found to be 172 pixels. The final conversion was found to be

$$\frac{5.25}{172}\frac{[\text{MeV}]}{[\text{pixel}]} \times 15.03\frac{[\text{mm}]}{[\text{MeV}]} = 0.46\frac{[\text{mm}]}{[\text{pixel}]}$$

The resolution in this experiment is approximately 30 KeV (1 pixel) based on a 300 dpi digitized image. Each time the camera position or lens is changed a

new energy vs pixel conversion must be calculated due to the change in image magnification.

Once the energy scale is set, actual energy measurements may be made with the single reference fiducial illuminated. The distance from this fiducial fixes the energy scale in the digitized photograph allowing the graticule lines to be left dark so as not to interfere with the raw data.

V. EXPERIMENTAL RESULTS

Pulserad data was recorded using a bellows camera set approximately 25 inches from the scintillator, a Geromac 1:6.8 f=220mm lens, and Type 57 Polaroid film. The camera was set up directly behind the energy analyzer in line with the input electron beam. Exposure was set at f/22 and all photographs were taken using an open shutter camera. The result is a time integrated energy measurement with scintillator brightness corresponding to total accumulated electron flux. When digitized, the resultant curve is a graph of accumulated electron flux vs energy. A typical curve is shown in Fig. 3 for Pulserad and Fig. 4 for SuperIBEX along with current and voltage waveforms derived from accelerator diagnostics (Fig. 5).

Six "shots" were taken using a $^1/_4$" diameter cylindrical cathode tip in the beam diode. Five "shots" were taken using a 1 $^1/_2$" diameter spherical cathode tip. In all cases the anode-cathode (A-K) gap of the beam diode was set at 18 mm, and the energy analyzer collimator gap was set at 1.25 mm. The potential across the A-K gap was calculated using Pulserad diode voltage and current diagnostics by correcting for diode inductance using the following relation:[7]

$$V_{gap} = V_{diode} - L\frac{\partial I_{diode}}{\partial t} \qquad \text{where } L = 330 \text{ nh}. \tag{7}$$

The A-K gap voltage at peak diode current was used to estimate beam energy as it left the diode. This should correspond to the brightest spot on the time integrated photograph. Figure 3 illustrates the time integrated energy profile for a typical Pulserad shot measured using the energy analyzer. Comparison of calculated beam energy with data taken from the energy analyzer for shots using the two cathode types is shown in Tables 2 and 3.

Shot Number	Current from Idiode (kA)	Energy from Vgap (MeV)	Energy from Analyzer (MeV)
Dragon		0.92	1.10
PR_218	14.2	0.75	1.32
PR_220	16.1	0.98	1.32
PR_224	12.5	0.83	1.46
PR_225	10.8	0.90	1.46
PR_227	8.8	1.05	1.48
PR_229	8.8	1.00	1.45
Ave		**.92**	**1.42**
Std Dev		.11	.07

Table 2 Pulserad shots using the Cylindrical Cathode design.

Shot Number	Current from Idiode (kA)	Energy from Vgap (MeV)	Energy from Analyzer (MeV)
PR_334			1.13
PR_335	14.2	.99	
PR_336	14.5	.95	1.10
PR_337			1.08
PR_338	15.3	.975	1.08
Ave		**.972**	**1.1**
Std Dev		.02	.02

Table 3 Pulserad shots using the Spherical Cathode design.

an: entries indicate that diagnostics were not available for that shot. The difference between calculated and measured energy is significantly higher for shots using the cylindrical cathode than it was for shots taken using the spherical cathode. This is most likely due to a change in the effective impedance of the Pulserad diode. The original cathode design for Pulserad presented a 50 Ohm load impedance to the Blumlein.[7] Changing to the cylindrical cathode altered the current density and electric field profiles in the diode. From energy analyzer data and Pulserad diode current waveforms, we find a 29% increase in beam energy and a 24% reduction in beam current when switching from the spherical cathode to the cylindrical cathode. Applying Ohms law to the diode voltage and current profiles shows that the average diode impedance found when using the cylindrical cathode is nearly double that found when using the spherical cathode.

In order to correct for the cylindrical cathode using Eq. (7) we must determine the effective inductance of the new diode. This would require a detailed knowledge of the diode field configuration. It could also be done by firing the accelerator into a short circuit so that V_{diode} will be zero and calculating the inductance given the $\partial I/\partial t$ from Pulserad diagnostics. Given a typical $\partial I/\partial t$ of 5 kA/ns, L would have to change by approximately 300 nH to account for the discrepancy between measured diode voltage and energy analyzer data. Variation in inductance based on changes in the cathode geometry should be much lower than this. It would appear that the Pulserad voltage monitor either fails at high diode impedances or simply fails near 1 MeV regardless of diode configuration. This clearly illustrates the utility of having an independent means for measuring beam energy.

The time integrated energy spectrum of SuperIBEX was also measured. The data was recorded using the same camera setup as was used previously with Pulserad. Figure 4 illustrates the data obtained. The energy measurement in this case is in close agreement with SuperIBEX diode voltage and current diagnostics.

VI. ERROR ANALYSIS

The major sources of error were examined to determine the impact on device accuracy. Numerical calculations for the device used in this experiment are included to give a feel for the numbers. The sources of error considered include errors due to:

1. Finite Slit Width - This affects the measured energy spread of the beam. The measured energy vs intensity curve for a beam with a finite energy spread is a convolution of the rectangular slit profile with the actual energy profile of the beam. To recover the true energy profile of the beam a deconvolution routine could be written. To estimate the uncertainty due to this effect note that with a 1.25 mm slit, a mono-energetic beam will appear as a 1.25 mm band of energies centered about the true energy of the beam. The resultant uncertainty is $.625\,\text{mm} \times 66.52\,\text{KeV / mm} \equiv \pm 42\,\text{KeV}$.

2. Beamlet Expansion - As the beamlet propagates within the keeper it will expand due to space charge forces and intrinsic emittance. Figure 6 shows the beamlet expansion factor $R = r_m/r_o$ vs distance for three different values of $\Delta\theta$. Here r_m is the radius of the beam edge at a given distance z along the semi-circular path from the collimator to the scintillator, r_o is the radius of the beam edge at the collimator, and $\Delta\theta$ is the beam emittance normalized by r_m. These curves apply for a collimator gap setting of 1.25 mm, a beam energy of 1.42 MeV, and a beamlet current density of 3 A/mm^2. Note that the largest $\Delta\theta$ a particle may possess and still pass through a collimator with this setting is 0.09 radians. For larger entry angles the particle will be blocked by the collimator and prevented from entering the keeper.

   The expansion can be significant at higher energies and for finite emittance. At 1.4 MeV, a zero emittance beamlet expands by 9%. This increases the apparent slit width, slightly increasing the slit energy spread from ±42 to ±45 KeV.

3. Digitization Process - The maximum accuracy to which the energy scale can be set is limited by the consistency with which we can measure a fixed distance in space using digitized photographic data. The result of multiple

trials placed this error at approximately 1%. The maximum resolution corresponds to 1 pixel, or 30 KeV.

4. Variation in Magnetic Field Strength - Detailed measurements of the magnetic field showed the error due to fringing fields and variation in static field strength to be < 2%.[2] This corresponds to an uncertainty in energy of approximately 20 KeV at the 1 MeV line.

   The static magnetic field in the energy analyzer was found to be 4.5 KGauss ± 0.3% using a Bell Hall probe, and the conversions used in calibrating the device assume this field strength. The error due to a variation in the static magnetic field can be estimated using Eq. (3). The expression for an incremental change in energy due to a variation in B_z is given by

$$\Delta E = 2C_1 r_c \frac{\Delta B_z}{B_z} \tag{8}$$

   where the value of the constant $C_1 = 66.52$ KeV/mm is fixed by the construction of the device. For an uncertainty in B_z of 0.3%, we get a ΔE of approximately 10 KeV at the 1 MeV line.

5. Stray Magnetic Field in Collimator - Any stray magnetic field inside the collimator will cause it to behave like an energy high pass filter. Electrons with an energy below a critical magnitude will be deflected into the far end of the collimator. Those not cut-off will enter the keeper with two components of velocity, one in the direction of beam propagation, and one transverse to the direction of beam propagation due to the magnetic field in the collimator.

   Measurements with a Bell Hall probe show the static magnetic field in the collimator to range from -33 to +58 Gauss with an average value of 35 Gauss. The cut-off energy due to stray magnetic fields in the collimator is found by solving for the effective cyclotron radius in the collimator (see Fig. 7). The result is a transcendental equation that can be solved numerically for z',

$$z' \cos^{-1}\left\{\frac{(z'-a)}{\sqrt{(z'-a)^2+\ell^2}}\right\} = \frac{\ell}{\cos\left[\tan^{-1}(a/\ell)\right]} \tag{9}$$

Recognizing that $z' = r_c$ and using Eqs. (3) and (5), the minimum kinetic energy a particle must possess to pass through the collimator without hitting the edges of the slit can be found. Figure 8 shows the relationship of cutoff energy vs collimator gap setting for two incident beams of different energy. Note that settings much below 1 mm will result in erroneous energy readings at the low end of the energy scale for low energy beams.

Those particles not cut off will pick up a transverse velocity component that will cause the particles to strike the scintillator at a larger than expected distance from the collimator, thus causing an erroneously high energy reading. A rough estimate of the error is found by calculating the worst case transverse velocity, v_T, occurring for a particle just above cutoff. This is given by the width of the collimator gap divided by the time spent in the collimator,

$$v_T = \frac{a}{t_c} = \frac{a}{\ell}\beta c = \frac{ac}{\ell}\sqrt{1-\frac{1}{\gamma^2}} \tag{10}$$

where the length of the collimator is fixed at l = 50 mm for this device.

An added force results from v_T,

$$\vec{F} = e\cdot\left[\left(\vec{v}_L \times \vec{B}\right) + \left(\vec{v}_T \times \vec{B}\right)\right] \tag{11}$$

This added transverse force is approximately $.015 v_T$ for a 1.42 MeV beam. Solving Eq. (1) with $\dot{r} \neq 0$ yields an expression for the cyclotron radius that takes into account the transverse velocity component. Assuming that $v_\theta \equiv r\dot{\theta}$ ($v_L >> v_T$), the revised expression for the cyclotron radius is given by,

$$r \cong \frac{\gamma m}{eB_z}\left(\beta c - \frac{\dot{r}}{\dot{\theta}}\right) \tag{12}$$

The difference in energy caused by the stray field in the collimator is given by

$$\Delta E = 2C_1\Delta r_c = 2C_1(r - r_c) = 2C_1 r_c\left(\frac{v_T/v_L}{1 + v_T/v_L}\right) \qquad (13)$$

where C_1 is the energy vs distance conversion found earlier and $2r_c = 21.075$ mm for the 1 MeV line in this device. We get a maximum error of approximately 21 KeV in this case.

6. Beam Collision with the Collimator - Grazing collisions with the collimator could alter the measured energy spread of the beam although electrons contacting the collimator are most likely scattered through large angles. The result will be a noise floor or haze in the photographic data that can be subtracted out without adversely affecting the data.

7. Bremsstrahlung - Collisions of energetic electrons with the wall of the keeper behind the scintillator could generate X-rays. Secondary electrons scattered from the keeper wall could pass through the scintillator again at a different position than that of the incident beam. Both of these factors would result in a larger than predicted energy spread without affecting the energy measurement. Further quantitative analysis may be indicated here.

8. Film Nonlinearities - Care must be taken to take photographic data at constant exposures as close as possible to the center of the film's linear operating range. This is another area ripe for further quantitative analysis.

9. Slit Centroid Position - Measurement of the distance from the slit to various positions on the scintillator was made from the far (fixed) edge of the slit. Since the slit width is finite, the actual distance from the slit (beamlet) centroid to a given position on the scintillator is closer by one half the slit width. This means that the actual beam energy is less than that calculated using the procedure outlined above. For this device using a 1.25 mm slit width, the energy measurement is 42 KeV higher than the actual beam energy.

The sources of error that result in a net shift in measured beam energy include the presence of a magnetic field in the collimator and shifting of the slit centroid position. These errors total approximately +60 KeV. None of the errors examined result in a net decrease in measured energy, the remainder affecting the beam energy spread only. This is in reasonably close agreement with the observed error in measured energy.

VII. CONCLUSION

The electron energy spectrometer has proven to be a useful device for measuring beam energy directly. Accuracy on the order of 100 KeV (10% at 1 MeV, 2% at 5 MeV) has been demonstrated and there are opportunities for improvement. For low energy measurements or when extreme accuracy is required processing could be done on the digitized data to deconvolve the finite slit width and beamlet expansion effects. The effects of stray magnetic field in the collimator and the movement of the collimator slit centroid are most easily compensated for by subtracted them from the energy measurement as the last step in the analysis. Increasing the size of the image on the film and/or increasing the number of dots per inch used in digitizing the image will decrease the error due to the digitization process as well as increase experimental resolution. Experimenting with film types promising greater dynamic range may also improve the accuracy and resolution of the energy measurement. Perhaps the best way to improve accuracy and resolution is through the use of streak cameras or framing cameras using CCD's. These last two methods would permit time resolved measurement of beam energy as well.

VIII. ACKNOWLEDGEMENTS

We would like to thank Dr. R. E. Pechacek for valuable assistance in perfecting the optical data collection system and Matthew Myers for assistance in running the Pulserad accelerator diagnostics. Thanks also go to Bill Dolinger and Gary Littlejohn for assistance in running the accelerator and machining parts used in this experiment. This work was supported by the Office of Naval Research.

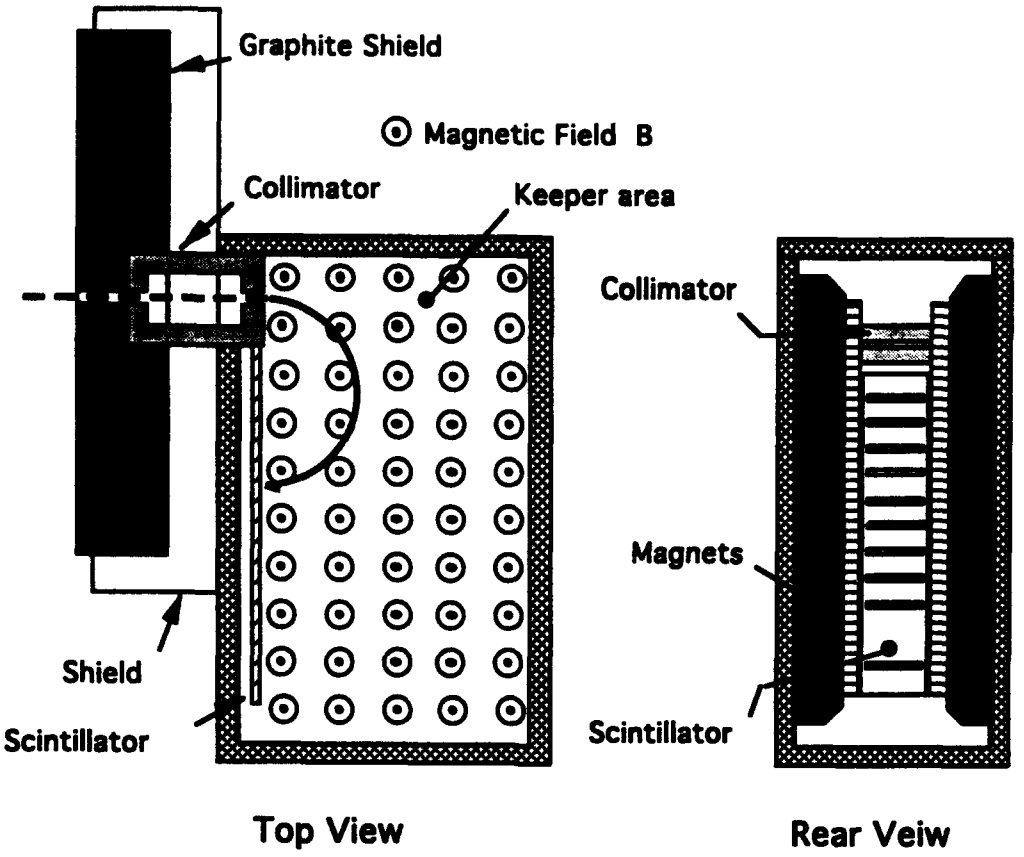

(a)

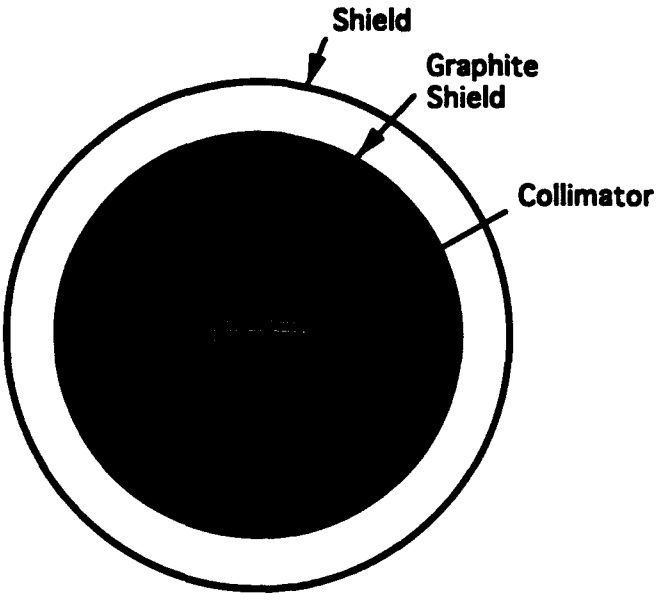

Front Veiw

(b)

Figure 1 Cutaway view of energy analyzer.

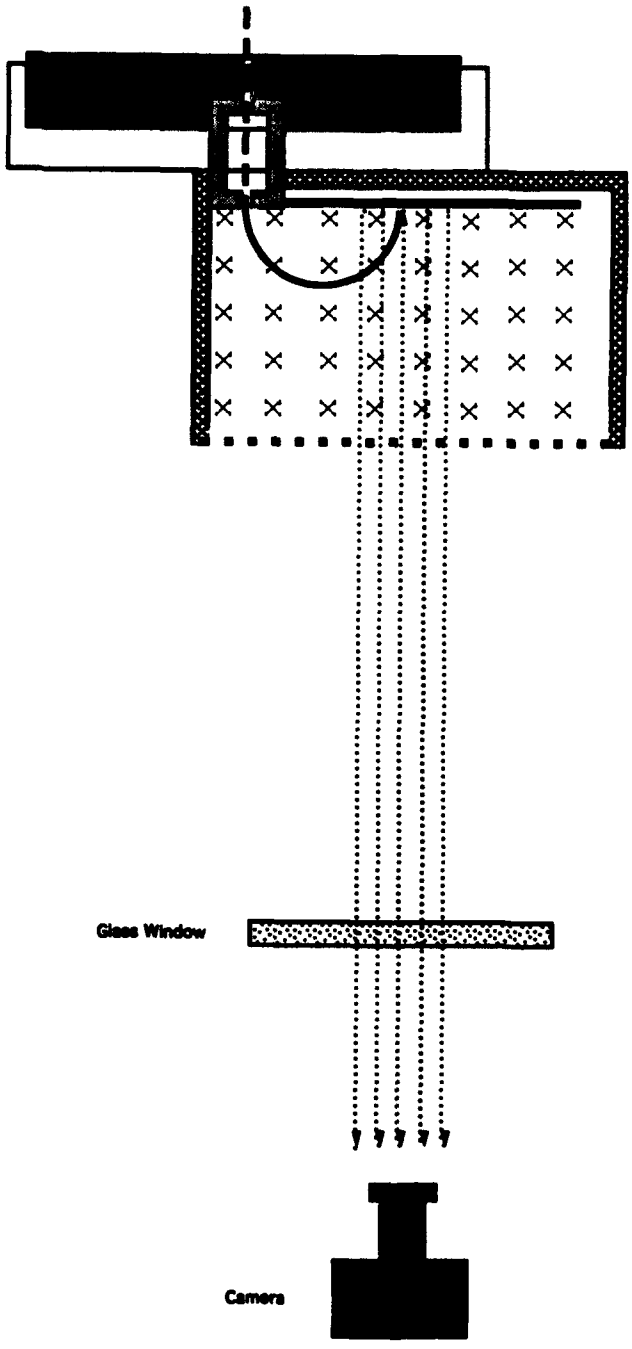

Figure 2 Experimental Setup.

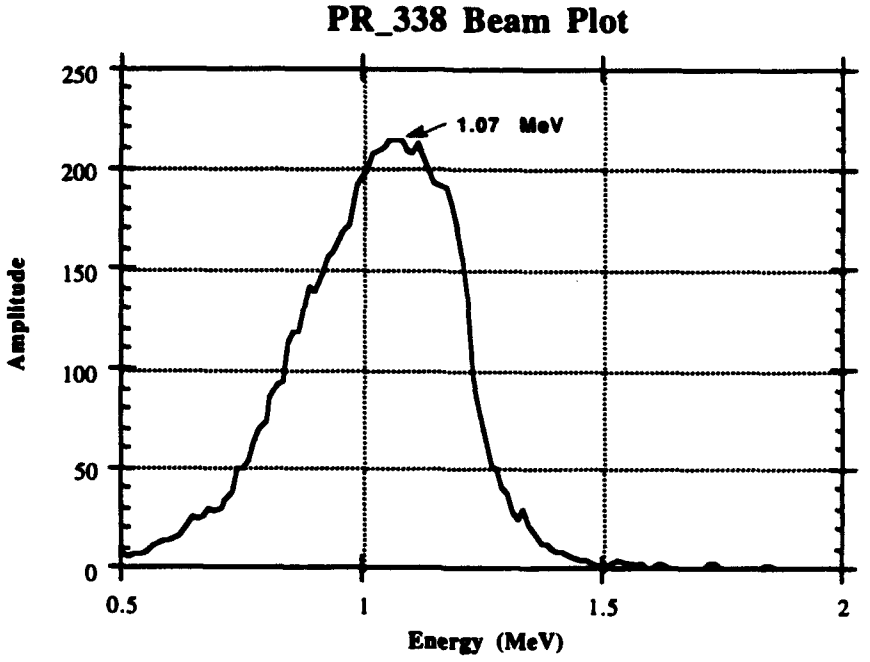

Figure 3 Typical Pulserad time integrated energy spectrum.

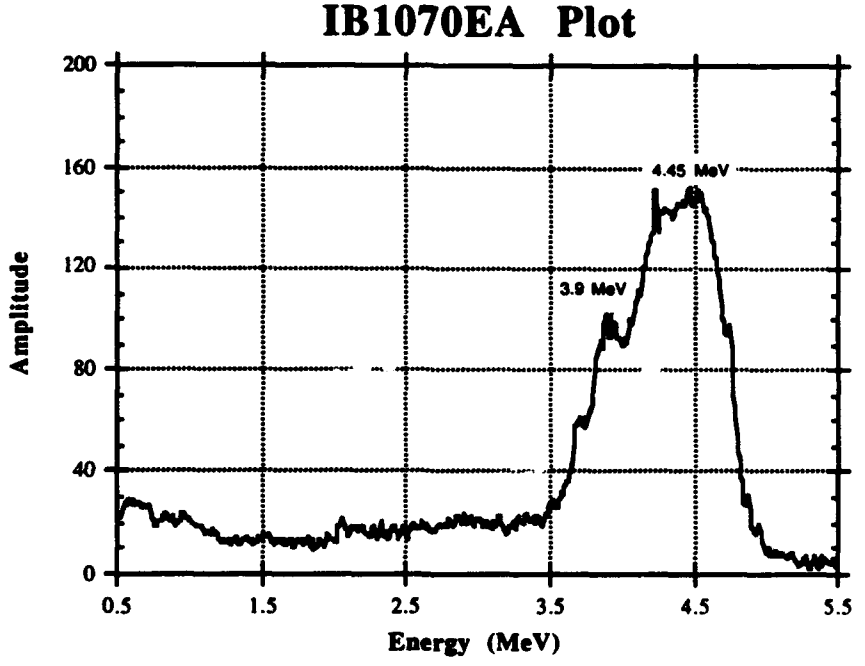

Figure 4 Typical SuperIBEX time integrated energy spectrum.

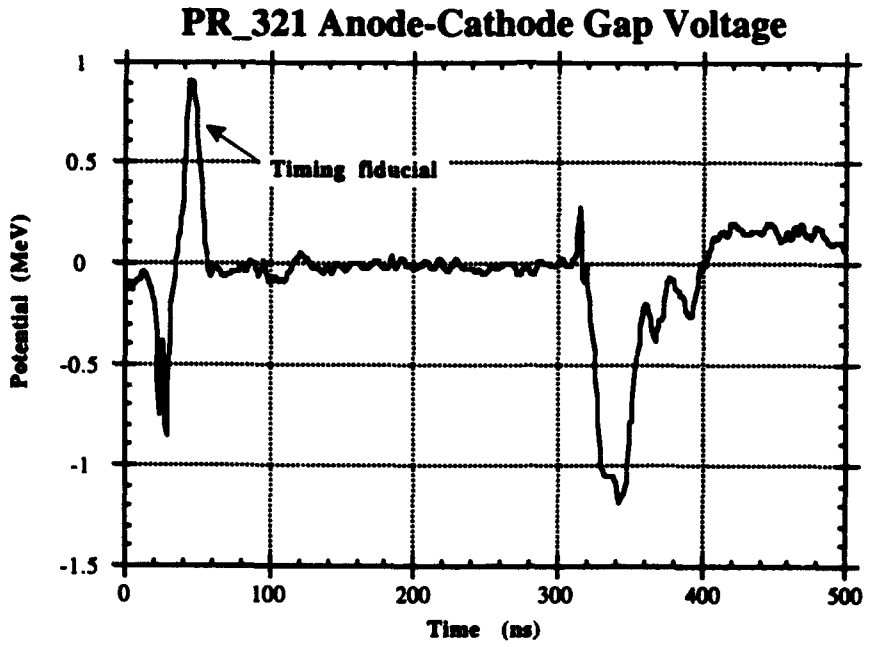

Figure 5(a) Typical Pulserad anode-cathode gap voltage trace.

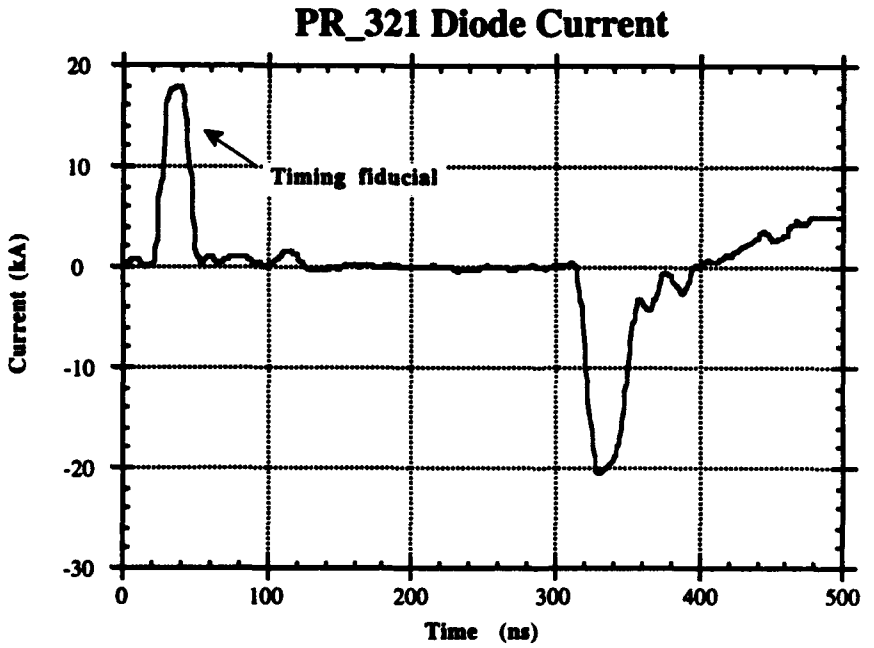

Figure 5(b) Typical Pulserad diode current trace.

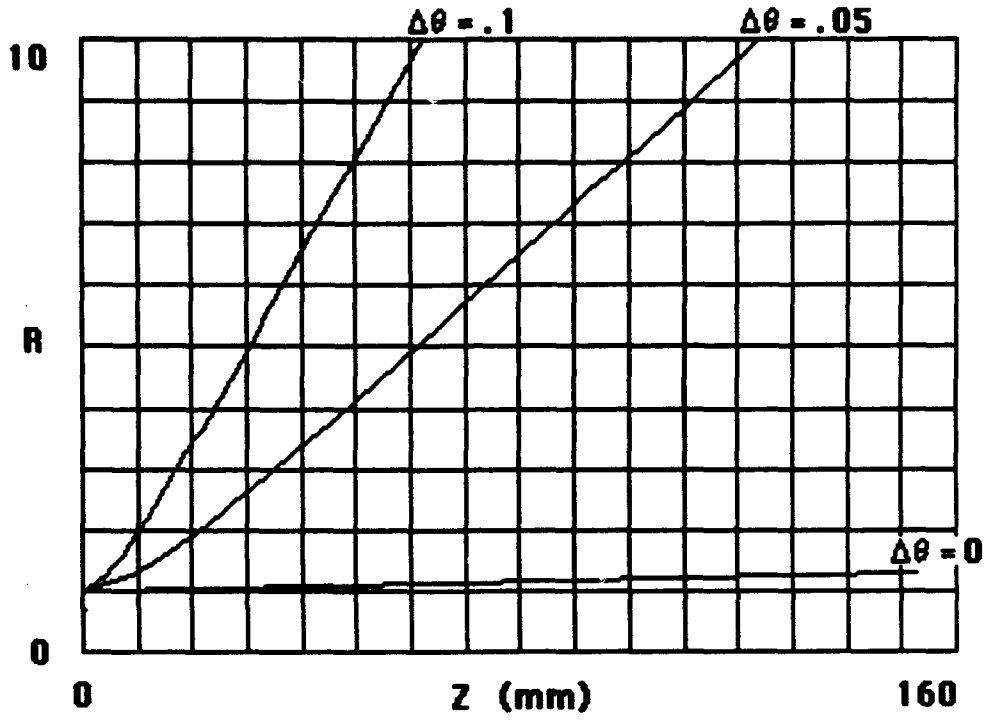

Figure 6 Beamlet expansion factor, S, vs distance z for $\Delta\theta = 0$, 0.5, and 0.1 radians.

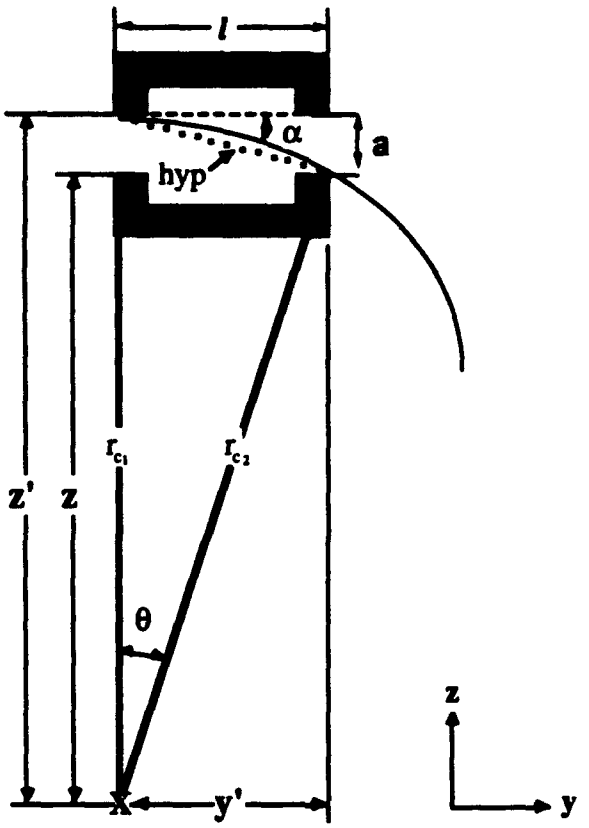

Figure 7 Geometry for collimator cut-off energy calculations.

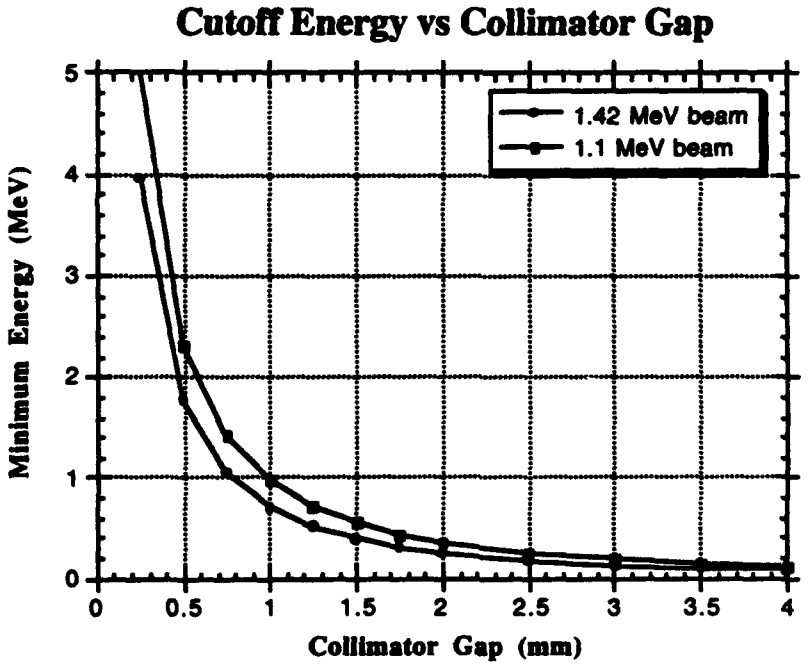

Figure 8 Graph of cutoff energy vs collimator gap setting.

IX. REFERENCES

1. "Experimental studies of an electron spectrometer and energy range measurements," University of Maryland Laboratory for Plasma Research, 1990.

2. P. Huang, "Experimental Studies of the Laser-Controlled Collective Ion Accelerator," Masters thesis, UMCP Department of Electrical Engineering, 1990.

3. R. F. Schneider, C. M. Luo, M. J. Rhee, and J. R. Smith, "Compact magnetic electron energy analyzer," Rev. Sci. Instrum. 56 (8), 1534-1536, (1985).

4. D. J. Weidman, M. J. Rhee, and R. F. Schneider, "Time resolving electron energy spectrometer," Rev. Sci. Instrum. 62 (2), 548-549, (1991).

5. R. L. Blondell, "Electron Spectrometer," UMCP ENEE 418 Project (Dr. W. W. Destler, Professor), 1989.

6. D. P. Taggart, D. P. Murphy, M. C. Nash, R. E. Pechacek, M. Raleigh, R. F. Schneider, R. A. Meger, "Relativistic Electron Beam Production Experiments at NRL," DARPA/Services Propagation Review, 1987.

7. J. A. Antoniades, D. P. Murphy, (private communication).

8. J. Gregor, "Electron Beam Energy Measurements using the UMCP-LPR electron spectrometer," Internal paper, CPB, 1991.

9. M. Reiser, Theory and Design of Charged Particle Beams, Manuscript to be published, 1993.